Supplementary Data Contents:

Supplemental Figure 16: Clone F9 specifically recognizes the integrin β8 subunit and stains human and not mouse β8 in formalin-fixed paraffin embedded (FFPE) tissue

Supplemental Figure 17: Clone F9 stains β8 in normal human epithelial and neural-derived cell types. F9 immunostaining of archival FFPE tissues

Supplemental Figure 18: Clone F9 does not stain β8 in stromal or immune cells in LLC tumors growing in humanized *ITGB8* BAC transgenic mice

Supplemental Figure 19: Full uncropped unedited immunoblot photomicrograph used for Supplemental Figure 15

Supplemental Table 1: Differentially expressed genes in tumor cells, tumor associated macrophages, CD8+, CD4+ T-cells

Supplemental Table 2: Gene Ontology Enrichment in tumor cells, tumor associated macrophages, CD8+, CD4+ T-cells

Supplemental methods:

Antibody Generation:

C6D4: We engineered a potent antibody that inhibits αvβ8-mediated activation of TGF-β to test the role of αvβ8 in cancer growth in preclinical murine models. To accomplish this, we sought to directly target an epitope shared by mouse and human within the ligand-binding pocket of αvβ8. We engineered a mutant αvβ8 integrin lacking the specificity-determining loop (SDL) of the human β8 subunit (a.a.195-222), which forms a key portion of the ligand-binding pocket and its primary sequence is entirely conserved between mouse and human (**Supplemental Figure 1A**). The SDL-deficient mutant was expressed as an αv-associated heterodimer on the cell surface and folded correctly, as antibodies to the β-head domain (clone 68) and Psi domain (clone F9) both bound efficiently to the SDL-deficient mutant αvβ8 receptor (**Supplemental Figure 1B**). The SDL was essential for ligand-binding and function since CHO cells expressing the SDL-deficient β8 mutant did not bind to a TGF-β peptide containing the RGD binding motif or support TGF-β activation (**Supplemental Figure 1C**). We used antibody engineering to create a recombinant antibody called C6D4, which bound to the SDL domain and was positioned to directly interfere with binding of L-TGF-β to αvβ8, as visualized using negative-staining electron microscopy (**Supplemental Figure 1D**).

Thus, *ITGB8* +/- mice maintained on C57B/6 were backcrossed to the LCR outbred strain to produce live born *ITGB8* -/- mice. Mice were immunized with recombinant human αvβ8 protein for the primary injection and then at 2 weeks and at 3 weeks prior to euthanasia. Approximately 5000 hybridomas were generated and screened for their ability to bind to αvβ8 in an enzyme-linked immunosorbent assay (ELISA). Results were confirmed by cell staining, and function blocking was determined with the use of a TGF-β bioassay. We identified 24 hybridomas that blocked the ability of the αvβ8 ectodomain to bind to the latency-associated peptide of TGF-β1 and blocked TGF-β activation in a TGF-β (TMLC) bioassay. Blocking antibodies were screened against the recombinant form of αvβ8 engineered to lack the specificity-determining loop (SDL) of the β8 head domain. Antibodies not binding the SDL-deficient αvβ8 were then selected. Of these, 8 hybridomas produced β8-specific antibodies that did not bind to the cells expressing the β8 SDL-deficient construct. Variable (V) genes from eight hybridomas were isolated, sequenced, and found to comprise seven V_H and eleven V_K genes that were unique but related. Each V gene was amplified under mutagenic PCR conditions, and a single-chain variable fragment (scFV) library was constructed by mixing the amplified cDNA and fragments joined using splice overlap. The library served as an amplification template using primers designed to complement rabbit IgG V_H or V_L vectors. Eleven distinct V_H genes and sixteen distinct V_K genes were identified after sequencing >100 random clones and transfected in 165 different combinations into 293 cells. The eight pairs that produced the best binders were determined by cell

staining and FACS analysis, and by measuring binding affinity for CHO cells expressing human αvβ8. These eight rabbit IgG V_H/V_K pairs were then used to create a new mutagenic scFV yeast display library that was inserted into a yeast expression library vector. Two high-affinity binders from this selection and affinity maturation step were identified and designated clone 29 and clone 44. Random mutation mutagenic libraries were next made from V_H and V_L genes of clones 29 and 44, and from these libraries the higher-affinity binding clones C6 and D4 were selected and sequenced. Mutations in the complementarity-determining regions (CDRs) of C6 V_H and D4 V_K were identified, and the two chains were combined to create the composite antibody C6D4.

C6D4 exclusively recognized αvβ8 and not αvβ1, αvβ3, αvβ5 or αvβ6 (**Supplemental Figure 1E**). C6D4 bound specifically to WT but not *itgb8* -/- mouse tracheal epithelial cells, demonstrating both its specificity and recognition of mouse β8 (**Supplemental Figure 1F**). C6D4 potently inhibited both αvβ8-mediated TGF-β activation, compared to an earlier generation allosteric anti-human specific αvβ8 inhibitory antibody, B5, which maximally inhibits only 60% of αvβ8-mediated TGF-β activation (**Supplemental Figure 1G**) (1). A Kinetic Exclusion Assay (KINEXA ®, Sapidyne Instruments, Inc., Boise, ID) was used to measure the binding affinity of C6D4 to the ectodomain of αvβ8. C6D4 bound in solution to the ectodomain of the αvβ8 integrin with an apparent affinity of 832 pM. Size exclusion chromatography and negative staining electron microscopy were performed essentially as previously described (1).

F9: We desired to create a robust, specific antibody suitable for staining human β8 in FFPE, to determine the cell-type distribution of αvβ8 in human tissues. We used antibody engineering create an antibody, clone F9. Thus, a yeast display scFV library was created using V-genes from hybridoma clones 6B9 and 4F1, a new clone 6B9.1 was selected from this library. A second yeast display scFV library was created using the V-genes of 6B9.1 and following random PCR mutagenesis, sixteen affinity-matured variants from this second library were characterized in terms of binding affinity and two clones C4 and D10 were transformed in to rabbit IgG format. Both reacted weakly with human β8 in formalin-fixed paraffin-embedded tissue. A third mutagenic scFV library was then created from the variable regions of C4 and D10 and inserted in a phage display vector (pHen) and displayed as scFv on the phage surface. The induced phage library was screened against formalin fixed immobilized αvβ8. After multiple rounds of selection, fifteen related phage clones were identified and the final clone F9 was chosen and transformed into IgG format and characterized for binding to formalin-fixed paraffin embedded tissues.

F9 recognizes a human-specific epitope that specifically stains cells transfected with αvβ8 but not mock transfected cells and strongly detects a band of the appropriate size on Western blot (**Supplemental Figure 15**). F9 stains formalin fixed paraffin embedded (FFPE) tissues of mice humanized for the β8

integrin subunit (1) but not wild-type mice (**Supplemental Figure 16**). The main tissues expressing β8 in the humanized mice are neural, epithelial (bronchial, pancreatic, bile duct, intestinal crypt, kidney glomerular podocyte) with no detectable expression in hepatocytes, myocytes, mesenchymal or immune cell compartments (**Supplemental Figure 16**). This pattern of distribution is reproduced in normal human tissues (**Supplemental Figure 17**).

Immunostaining protocol:

Tumor immunostaining: Formalin-fixed paraffin-embedded (FFPE) tissue sections were deparaffinized, and antigen retrieval was performed using either 0.4% (2)sin (#P-7125, Sigma) at 37°C for 5 min in a water bath, a Tris-EDTA buffer, pH 9.0 in a pressure cooker (97°C for 20 min), Reveal Declocker (Biocare Medical, Pacheco, CA) in a pressure cooker (95°C for 20 min), or a combination of pepsin and Reveal Decloaker steps, followed by treatment with peroxidase blocker (K4007, Dako). Non-specific binding was blocked with protein blocking solution (X0909, Dako) and Avidin/Biotin Blocking kit (004303, Thermo Fisher Scientific). Sections were stained with anti-mouse β8 (clone F9), B5 (anti-human β8 which does not work in FFPE immunostaining and thus used as isotype control), PD-L1 (E1L3N®) XP® Rabbit mAb (CST#13684) at 1:200 dilution in TBS with 0.05% Tween-20 overnight a 4°C. E1L3N® has been shown to produce concordant staining with 22C3 the FDA approved companion diagnostic to pembrolizumab , CD31 (NB100-2284, Novus Biologicals, Littleton, CO), Ki-67 (00375, Bethyl Livingston, TX), CD4 (14976682, ebioscience, San Diego, CA), CD8 (14080882, ebioscience) , F4/80 (MCA497B, BioRad, Hercules, CA) followed by detection with Biotin-SP conjugated anti-rat IgG (Jackson ImmunoResearch, West Grove, PA 712-065-153), anti-rabbit HRP (K4003, Dako), or streptavidin-HRP and DAB detection, as appropriate. TUNEL was performed according to the manufacturer's instructions (G3250, Promega, Madison, WI). For F9, the slides were additionally stained with labeled polymerase-HRP anti-mouse (Dako K4003) for 1 hr at RT, washed, and treated with Tyramide signal amplification solution A at a dilution of 1:100 (Life Technologies) according to the manufacturer's instructions. For PD-L1, stained slides were additionally treated with SignalStain®Boost IHC detection reagent (CST#8114) for 1 hr at RT.

Immunohistochemical scoring: All samples were blinded as to group, isotype, or test antibody. Digital images of blinded tumor groups were taken (Spot Imaging) and assessed for staining. For human samples, digital images of isotype or F9/PD-L1 were taken (5/tumor at 200x) and assessed for F9 and PD-L1 positivity using PD-L1 scoring criteria (3). Briefly, tumor cells with membrane staining were counted and compared to numbers of tumor cells without membrane staining and tumor proportion score (TPS) determined as stained cells/total tumor cells (4). Ambiguous staining results (i.e. faint membrane staining, or heavy background) were resolved by comparison to isotype stained slides. For mouse tumors, vascular

density (number of vessels/field) and vessel branch points (branch points/mm^2) were determined as described (5). Tumor infiltrating lymphocytes were assessed from 5 random digital images (Spot Imaging) taken from the periphery or central area of each tumor. The periphery of the tumor was defined as areas stained with ink prior to fixation and embedding, and/or showing entrapped adipocytes, skeletal muscle or skin appendages, and the central area defined as areas at least three contiguous 200X magnification fields from the periphery. The mean immune cell count was determined from cell number/mm^2, as described (6).

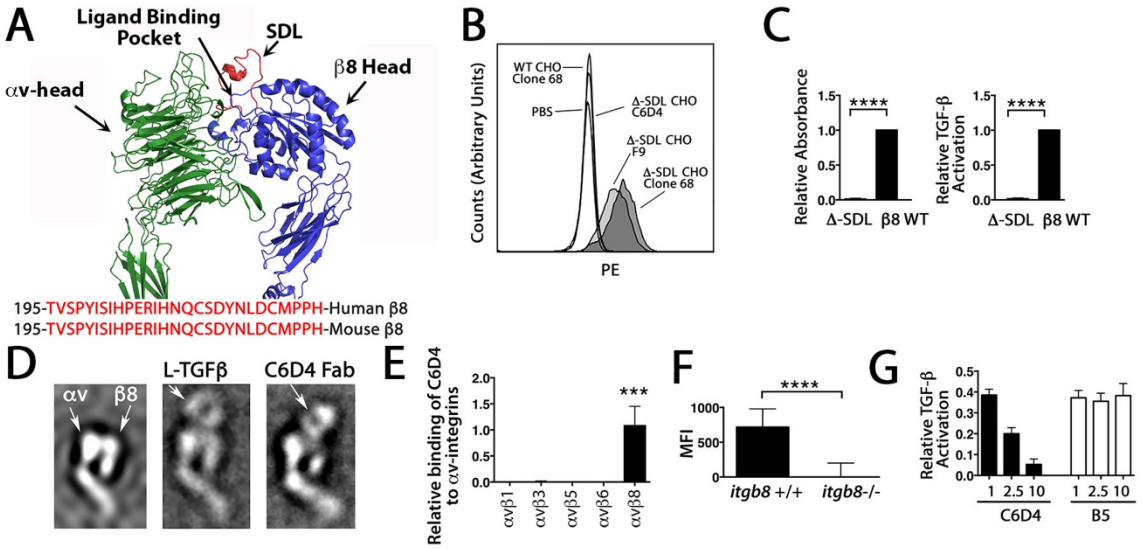

Supplemental Figure 1: The antibody C6D4 binds to the ligand-binding domain of mouse and human αvβ8 and effectively inhibits L-TGF-β binding to αvβ8 **A)** Ribbon model of the αvβ8 headpiece homology-modeled (Chimera v1.12) from the αvβ3 crystal structure [Protein Data Bank (PDB) 3IJE](7) showing the αv-(green) and β8-(blue) head domains and the β8-specifity determining loop (SDL, red) forming a portion of the ligand-binding pocket. Depiction rendered in PyMOL (PyMOL v1.8.4.0). The position and amino acid sequence of mouse and human SDL are shown below in red typeface. **B**) A mutant construct lacking the β8-SDL (Δ-SDL) was heterologously expressed on CHO cells and was recognized by domain specific antibodies (Clone 68, βI domain; F9, Psi domain) but not the anti-β8 antibody, C6D4, which was engineered to bind to the β8 SDL. **C**) The ability of CHO cells expressing Δ-SDL to adhere to a peptide derived from the TGF-β3 integrin binding motif (**left panel**) or to mediate TGF-β activation in a TGF-β bioassay (**right panel**) were compared to CHO cells expressing wild-type (WT) β8. Results were normalized to expression levels as shown in **B**. **D**) Class averages of negative-staining electron microscopy of the purified αvβ8 ectodomain alone (**left panel**), with bound L-TGF-β (**middle panel**), or with a fragment of antigen binding (Fab) of C6D4 (**right panel**). **E**) C6D4 binds exclusively to αvβ8. Soluble αvβ1, αvβ3, αvβ5, αvβ6, or αvβ8 were immobilized on ELISA plates (1 μg/ml) and C6D4 binding assessed by sandwich ELISA. Shown in binding relative to BSA coated wells. **F**) C6D4 binds to β8 expressed by mouse tracheal epithelial cells derived from WT (*itgb8*+/+, n=6) but not from *itgb8* -/- mice (n=3). **G**) C6D4 blocks αvβ8-mediated TGF-β activation by CHO cells stably transfected with a β8 expression construct. C6D4-mediated inhibition TGF-β activation was compared to an allosteric anti-human β8 antibody, B5, which maximally blocks 60% of TGF-β activation (1). All Experiments were repeated a minimum of three times. *p<0.05, **p<0.01, ***p<0.001, ***p<0.0001 as determined by unpaired Student's t-test.

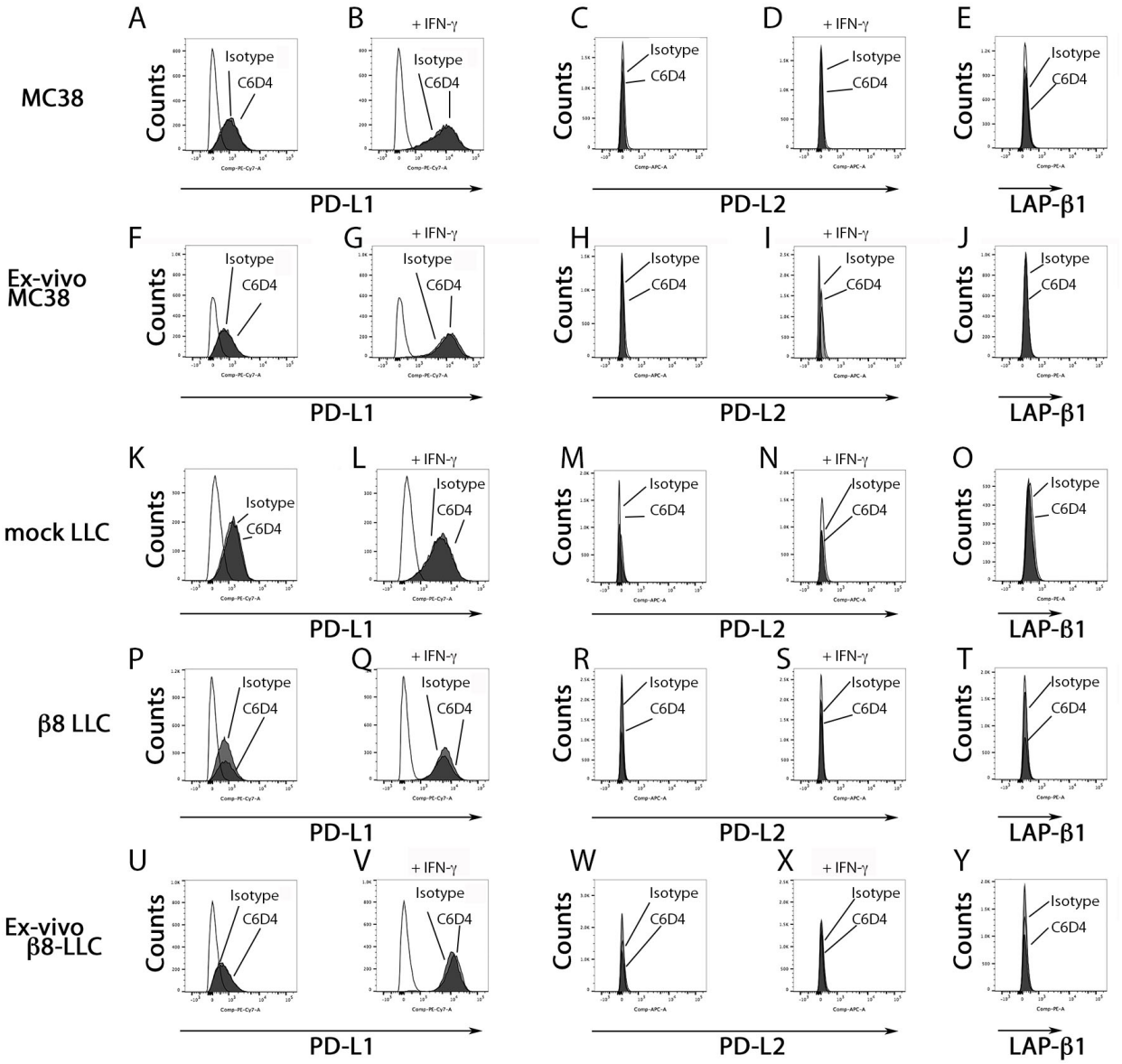

Supplemental Figure 2: Expression of PD-L1, PD-L2 and L-TGF-β on MC38 and LLC cells MC38 Cells (**A-E**) or MC38 cells isolated from tumors (**F-J**), Mock transfected (**K-O**), β8 LLC (**P-T**) or β8 LLC cells isolated from tumors (**U-Y**) were stained for **A, B, F, G, K, L, P, Q, U, V**) PD-L1; **C, D, H, I, M, N, R, S, W, X**) PD-L2 ; and **E, J, O, T, Y**) LAP of L-TGF-β1 24 hr after treatment with isotype control (light grey) or C6D4 (dark grey). **B, D, G, I, L, N, Q, S, V, X**) MC38 or β8 LLC were treated for 24 hr with recombinant IFNγ (10 ng/ml)and isotype control (light grey) or C6D4 (dark grey) and stained for PD-L1. Histogram overlays are shown with control antibody stained cells indicated by unfilled histograms. Shown are representative histograms from at least 2 experiments ($n \geq 8$ mice/group).

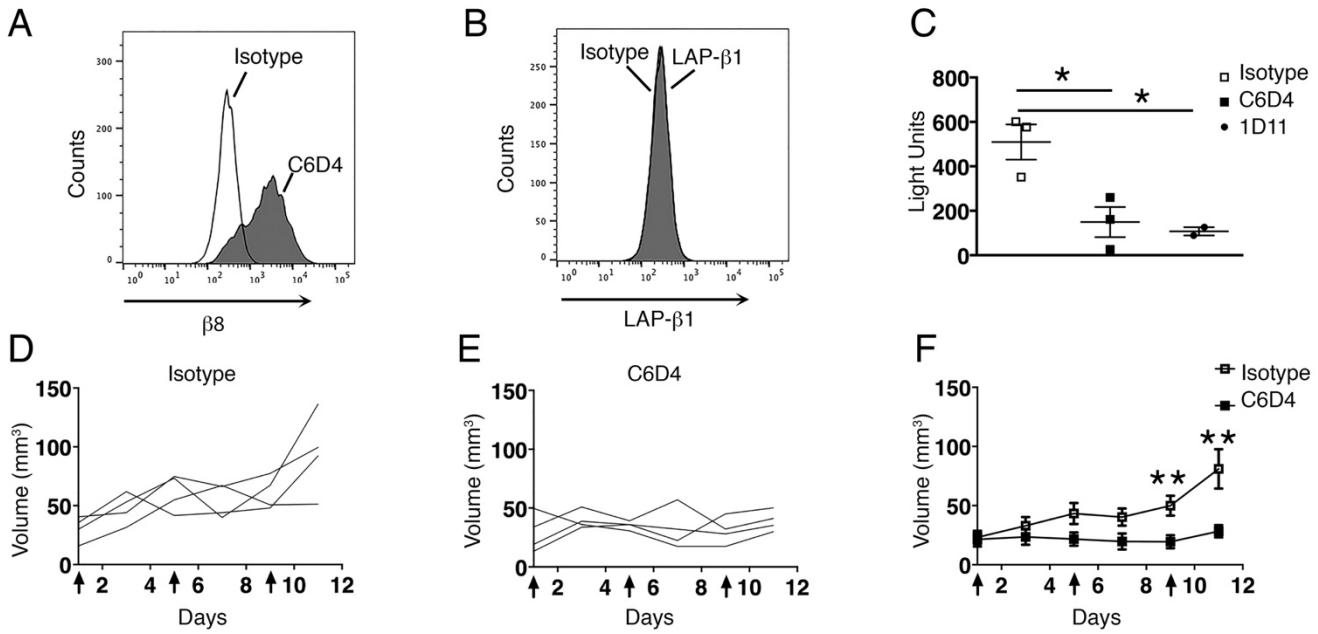

Supplemental Figure 3: TRAMP-C2 tumor growth is significantly inhibited by C6D4 **A**) The murine prostatic adenocarcinoma line TRAMP-C2 expresses αvβ8. TRAMP-C2 cells were stained for αvβ8 using C6D4 (filled). Staining was compared to isotype stained TRAMP-C2 cells (open). Shown is a representative experiment of 3. **B**) The murine prostatic adenocarcinoma line TRAMP-C2 does not express cell surface latent TGF-β1. TRAMP-C2 cells were stained for latent TGF-β1 using an antibody to the latency associated peptide (LAP) of TGF-β1 (filled). Staining was compared to isotype stained TRAMP-C2 cells (open). The histograms are superimposable indicating no detectable latent TGF-β1 expression. Shown is a representative experiment of 3. **C**) TRAMP-C2 cells in culture activate TGF-β. TRAMP-C2 cells were co-cultured with TMLC TGF-β reporter cells in the presence of isotype (open squares), C6D4 (filled squares) or 1D11(filled circles). All antibodies used at 10 μg/ml. Activation is shown in arbitrary light units. Shown is an average of three experiments repeated in triplicate. **D-F**) TRAMP-C2 cells (10×10^6) were injected into the flank of male C57BL/6 mice and after 17-19 days mice with palpable tumors were treated with **D**) C6D4 or **E**) isotype control (SV5) on days 0, 5 and 9 (7 mg/kg I.P.) as indicated by arrows. Shown are representative spider plots (**D-E**) of a representative of two experiments. In **F**) shown are tumor volume averages over time from two pooled experiments (n=8/group). Arrows indicate antibody injection days. **$p<0.01$ by two-sided unpaired Student's t-test

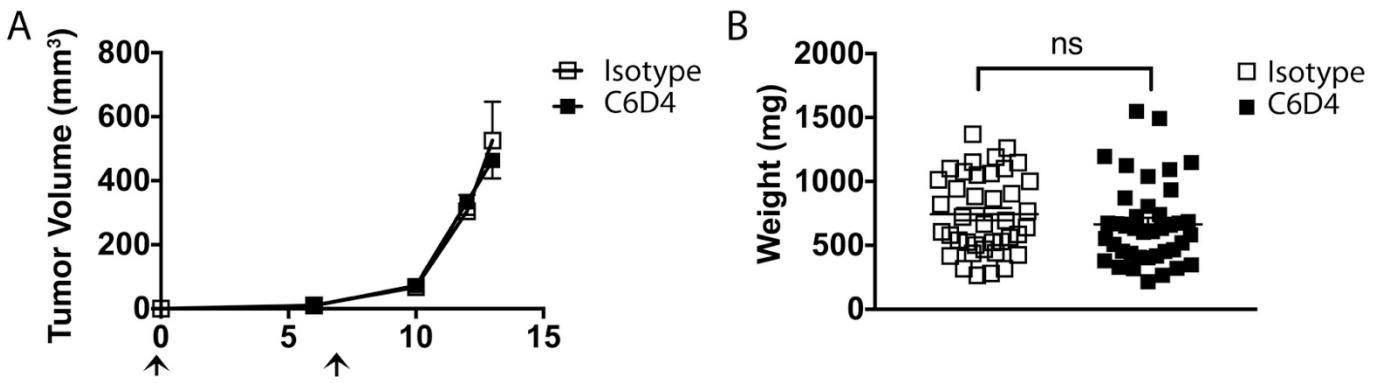

Supplemental Figure 4: Host cells expressing αvβ8 do not affect wild-type LLC tumor growth Wild-type LLC cells were injected subcutaneously into female C57BL/6 mice and mice were injected with isotype control antibody or C6D4 (7 mg/kg I.P.) on days 0 and 7 (arrows). **A**) Average tumor volumes from a representative experiment of 4 (open squares, isotype, n=9; filled squares, C6D4, n=11). **B**) Individual tumor weights (day 14) depicted in scatterplot from 4 independent experiments from mice treated as shown in **A**. Open squares, isotype, n=40; filled squares, C6D4, n=40).

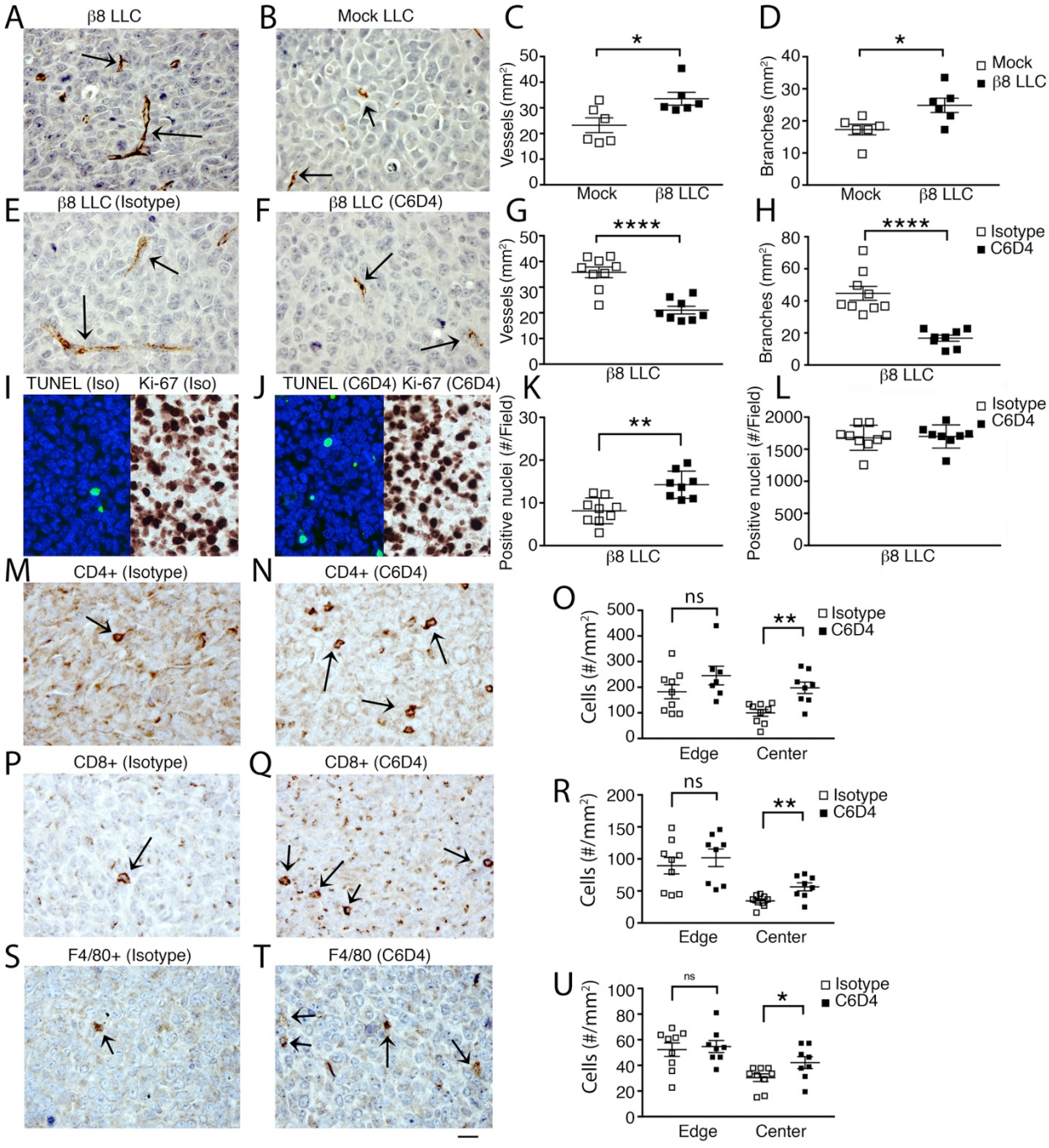

Supplemental Figure 5: αvβ8 expression increases LLC tumor vessel growth, tumor cell survival and immune exclusion **A)** β8 LLC tumors or **B**) mock- LLC tumors were stained with anti-CD31 and **C**) vascular density and **D**) vessel branching assessed morphometrically. β8 LLC tumors from mice treated with isotype (**E**) or C6D4 (**F**) were stained with anti-CD31 and **G**) vascular density and **H**) vessel branching assessed morphometrically. β8 LLC tumors from mice treated with isotype (**I**) or C6D4 (**J**) were stained by TUNEL (left panels) or Ki-67 (right panels) and assessed for apoptosis (**K**) or Ki-67 proliferation index (**L**). β8 LLC tumors from mice treated with isotype (**M, P, S**) or C6D4 (**N, Q, T**) were stained with anti-CD4 (**M**, **N**), anti-CD8 (**P, O**), or anti-F4/80 to stain macrophages (**S, T**). Representative positively stained immune cells are indicated by arrows. Quantification at tumor edge or center from individual mice for CD4 (**O**), CD8 (**R**) or F4/80 (**U**) are shown. n ≥8. Significance was determined by unpaired Student's t-test *p<0.05, **p<0.01, *p<0.001, ****p<0.0001

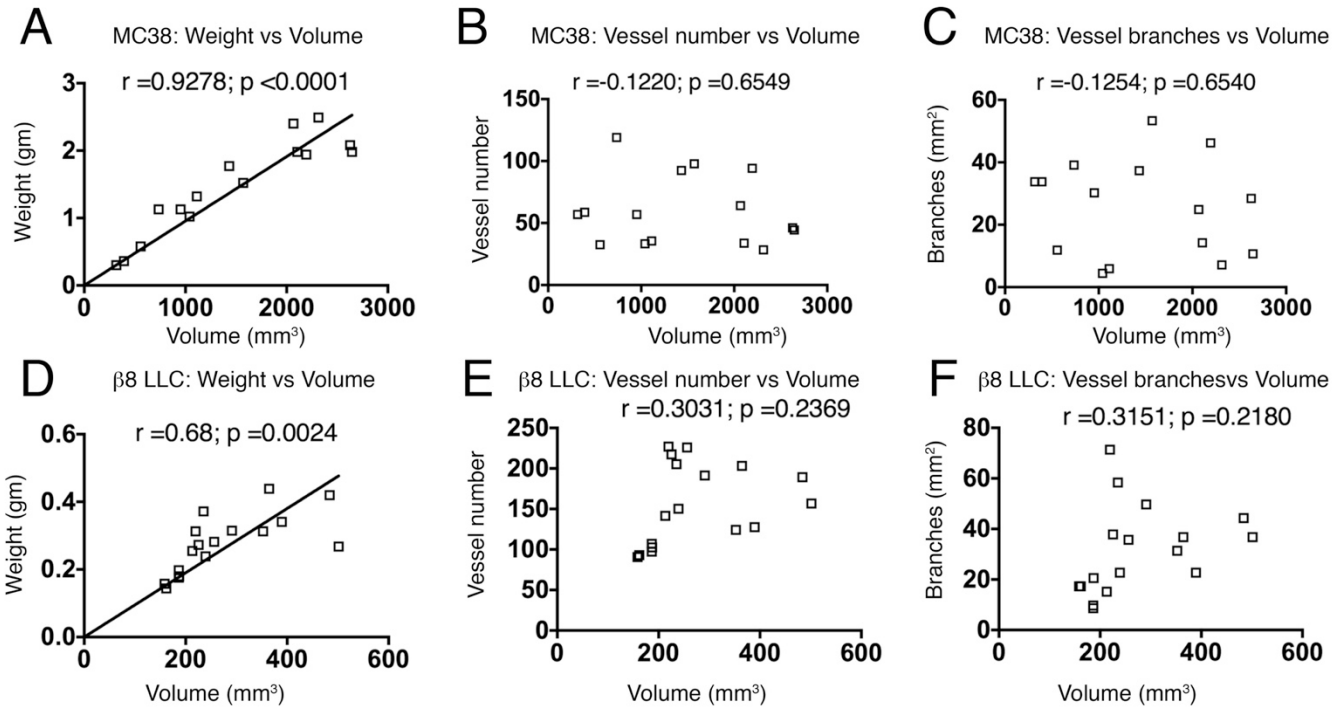

1

2 **Supplemental Figure 6: Vessel growth is independent of tumor size** Tumor volumes of MC38 (**A-C**) and
3 β8 LLC tumors (**D-F**) harvested from mice in a representative experiment shown in **Figure 3** and **Supplemental**
4 **Figure 5** were compared with **A, D**) tumor weight, **B, E**) vessel density and **C, F**) branch points/mm^2. Above each
5 graph are the Pearson r and corresponding p value. Only tumor weight is significantly correlated with volume.

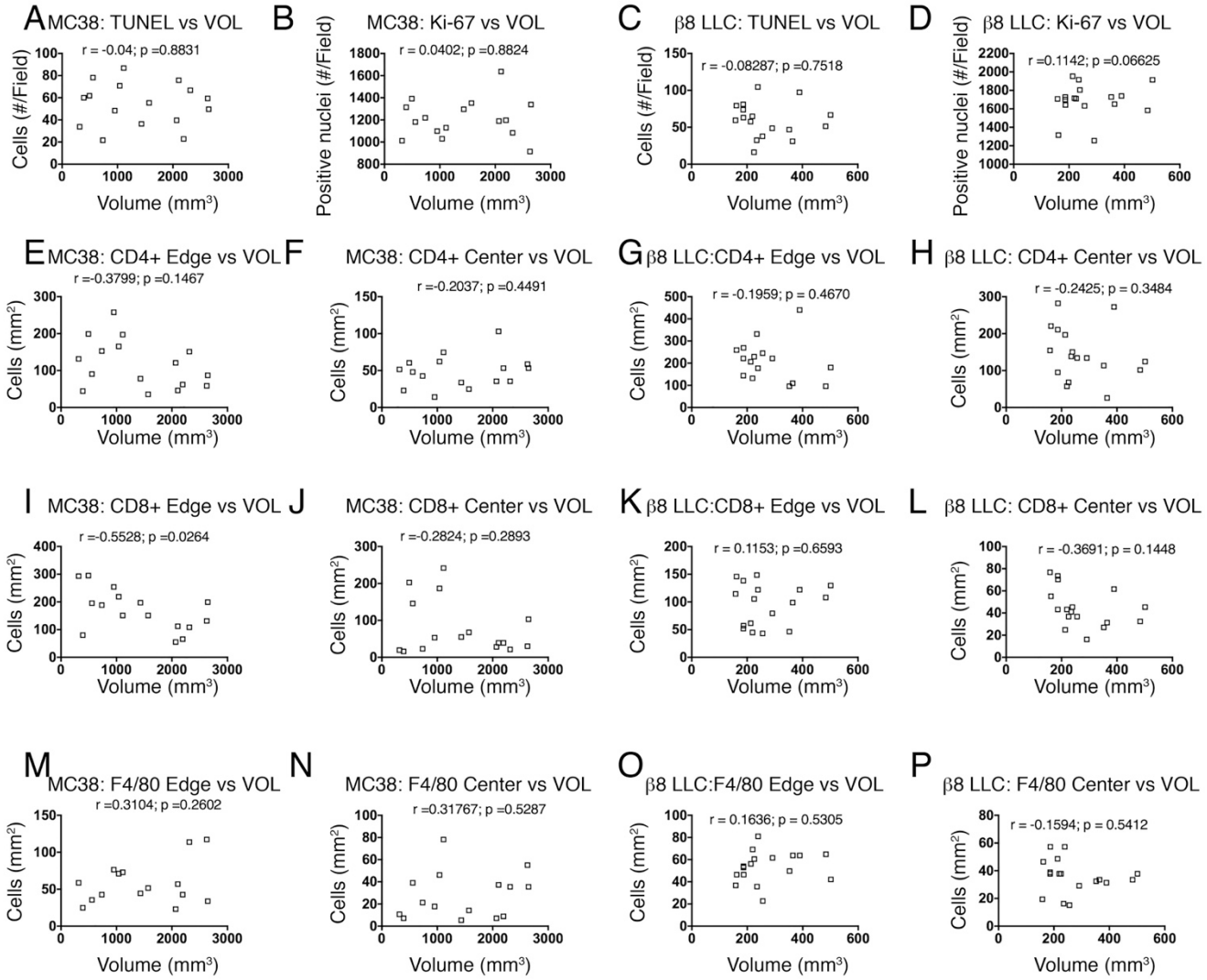

Supplemental Figure 7: Apoptosis, proliferation and immune cell localization are not correlated with tumor size Tumor volumes of MC38 (**A, B, E, F, I, J, M, N**) and β8 LLC (**C, D, G, H, K, L, O, P**) tumors from mice in a representative experiment shown in **Figure 3** were assessed for correlation with **A, C**) TUNEL positive cells/HPF, **B, D**) Ki-67 positive cells/HPF, **E, G**) CD4+ cells at the tumor edge or **F, H)** center. **I, K**) CD8+ cells at the tumor edge or **J, L**) center. **M, O**) F4/80 positive cells at the tumor edge or center **N, P**). Above each graph are the Pearson r and corresponding p values. None of the endpoints correlate with volume.

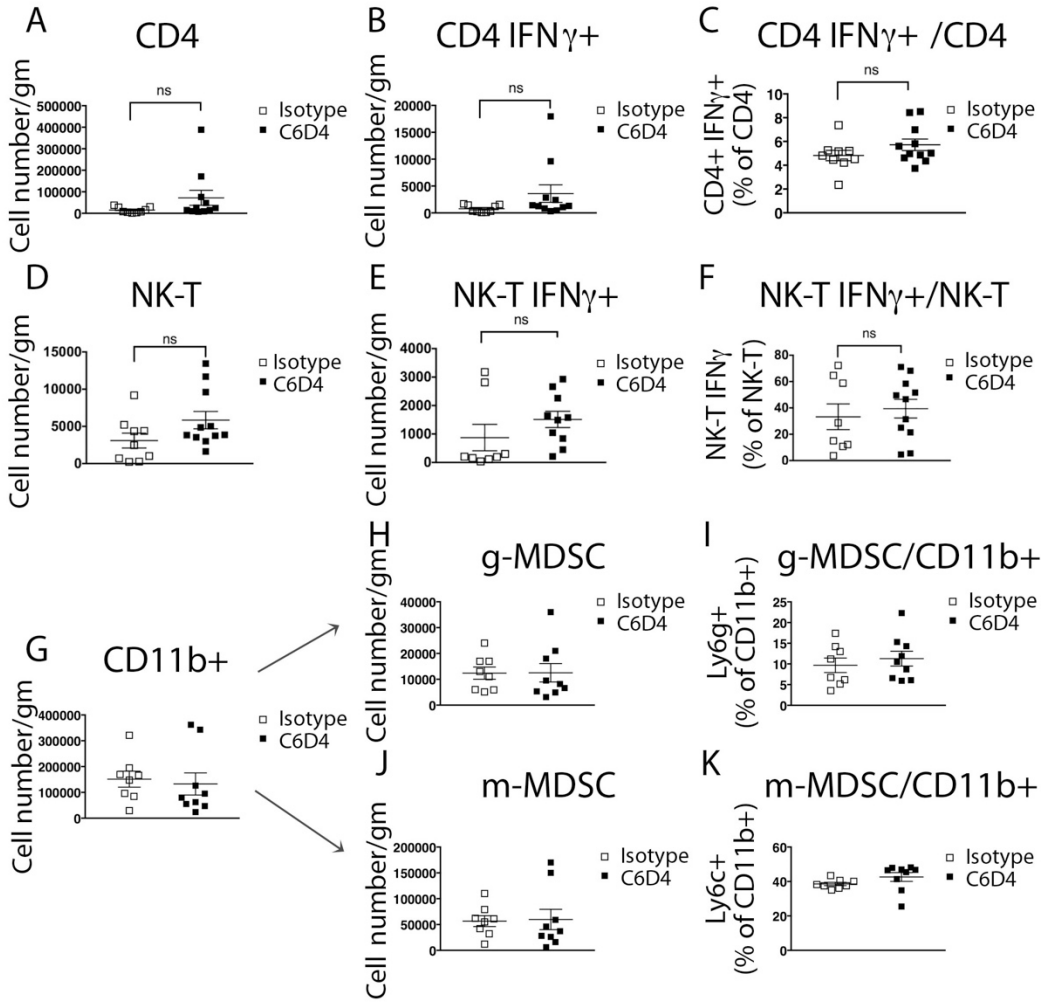

Supplemental Figure 8: IFNγ secreting CD4+ or TCRβ+ NK1.1 + or MDSC cells are not significantly increased in β8 LLC tumors from C6D4 treated mice Tumor infiltrating lymphoid cells from β8-LLC tumors harvested at day 14 post injection from mice treated with isotype or C6D4 (7 mg/kg) on days 0 and 7 underwent multicolor cell staining and analysis. Tumor associated lymphoid cells isolated from tumors from mice treated with isotype (open boxes) or C6D4 (closed boxes) are stained to identify numbers of CD4+ T-Cells (**A**) and IFNγ secreting CD4+ T-Cells (**B**), which were enumerated by size, CD45+, TCRβ+, NK1.1-, CD4+, IFNγ surface capture positivity relative to an isotype control (**A, B**) and percentages determined (**C**). Numbers of NK1.1+ TCRβ+ NK1.1+ "like" T-cells (**D**) were similarly identified and numbers (**E**) and percentages of IFNγ secreting (**F**) cells determined. CD45+ CD11b high cells were separated in Ly6g negative and positive (g-MDSC) populations. Ly6g negative cells were separated into Ly6c negative and positive (m-MDSC) populations, as described (8). The Ly6c negative population was further separated into F4/80 positive populations and then separated into CD11c positive MHCII high and low populations, as described (9).

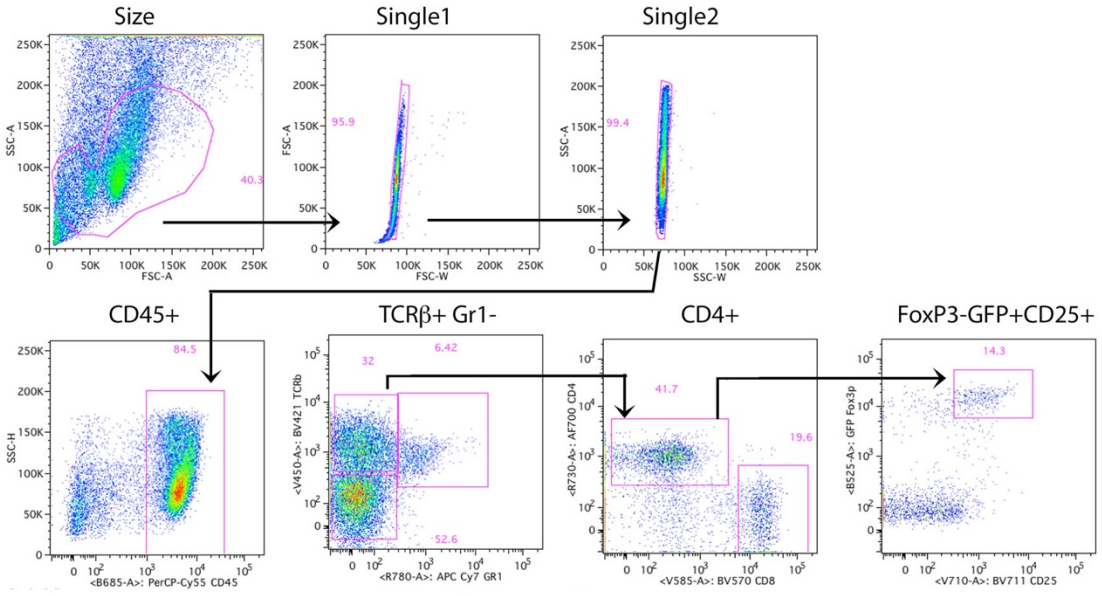

Supplemental Figure 9: Gating strategy for CD4+ Treg cells β8 LLC tumors were established in C57BL/6 mice expressing GFP inserted into FoxP3 downstream of the endogenous Foxp3 STOP codon (B6.Cg-Foxp3tm2Tch/J). Tumor infiltrating lymphoid cells harvested from β8-LLC tumors at day 14 post injection from mice treated with isotype or C6D4 (7 mg/kg) on days 0 and 7 underwent multicolor cell staining and analysis. Gating strategy is shown to isolate CD45+ TCRβ+ CD4+ FoxP3-GFP+ CD25+ cells.

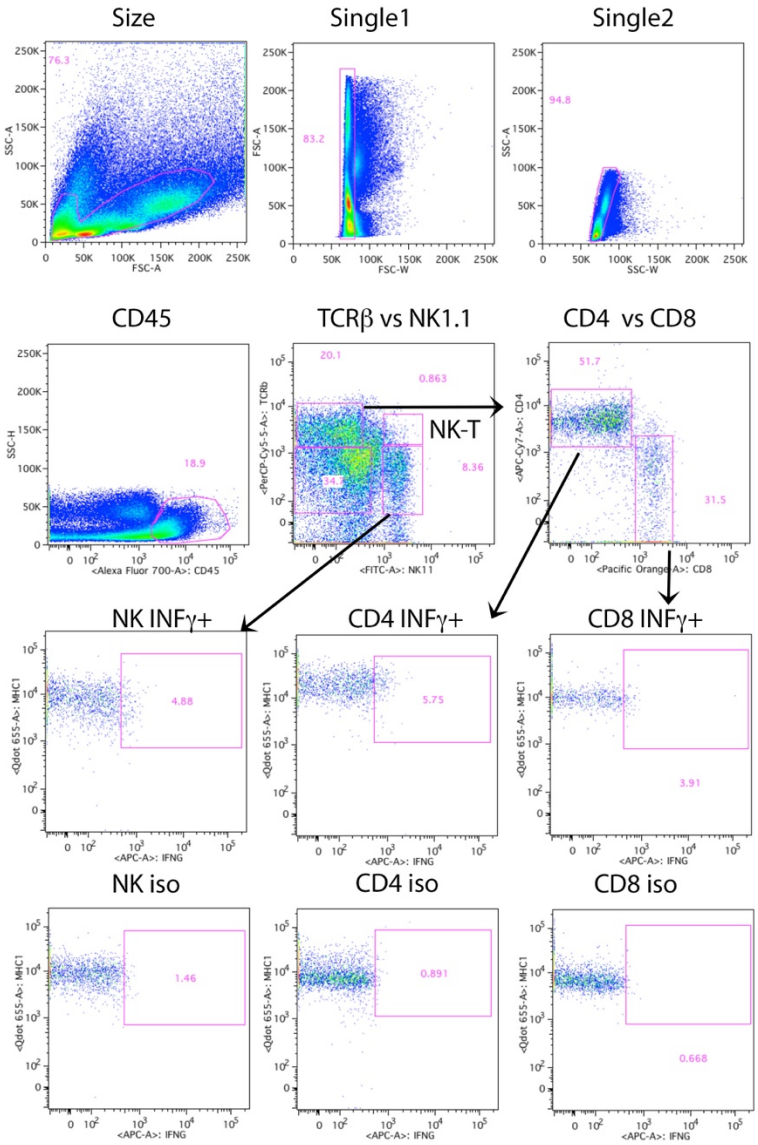

Supplemental Figure 10: Gating strategy for IFNγ secreting CD4+, CD8+ T-cells, and NK1.1+ cells
Tumor infiltrating lymphoid cells from β8-LLC tumors harvested at day 14 post injection from mice treated with isotype or C6D4 (7 mg/kg) on days 0 and 7 underwent multicolor cell staining and analysis. Show is a representative gating strategy to isolate CD45+ populations expressing either TCRβ, NK1.1 or both and the secretion of IFNγ by the NK1.1+ TCRβ- subset, the TCRβ+ NK1.1-CD4+ subset and the TCRβ+ NK1.1-CD8+ subset. The IFNγ shifts are similar as described for surface capture assays of stimulated ex vivo peripheral blood mononuclear cells (10). The shifts shown above represent 1 hr of cytokine secretion from freshly isolated *unstimulated* ex-vivo tumor associated immune cells.

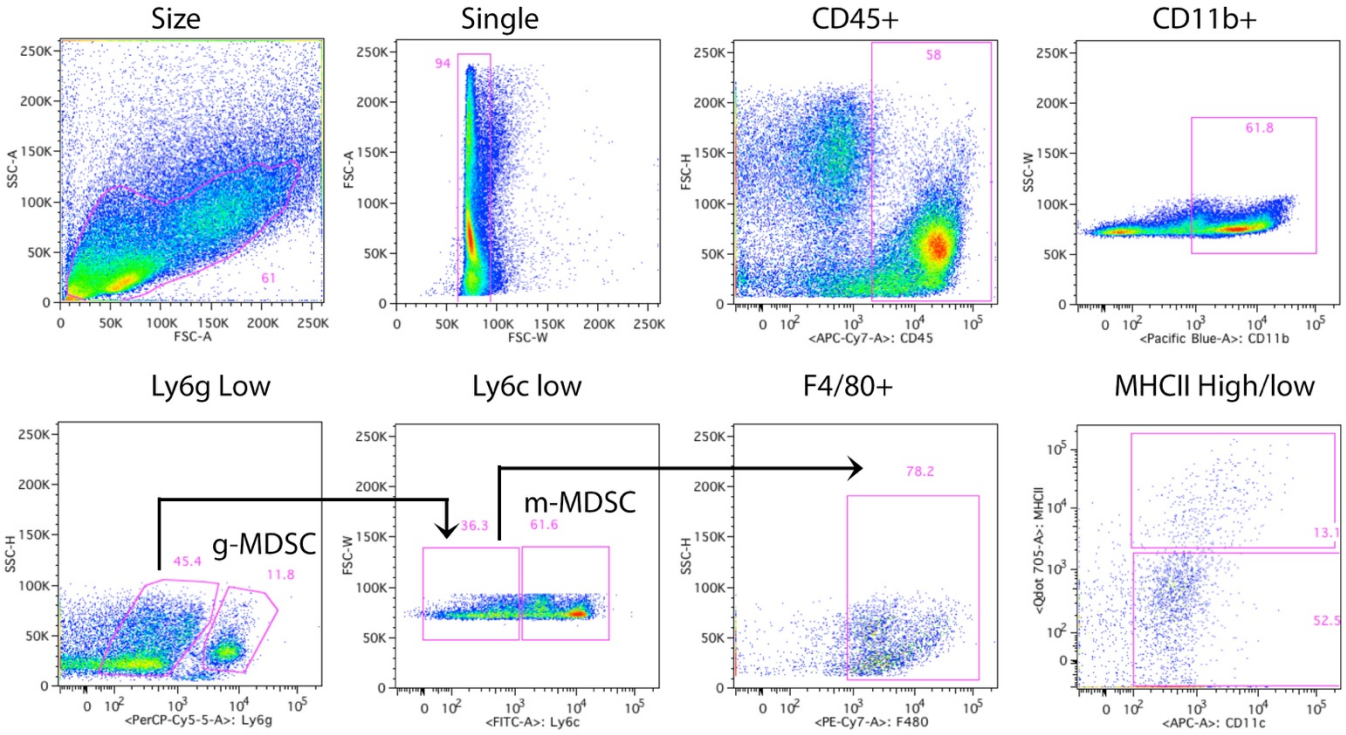

Supplemental Figure 11 Gating strategy for tumor-associated macrophages, g-MDSC and m-MDSC
Tumor associated macrophages (TAM) are a heterogeneous cell population that have been separated from resident macrophages by surface expression of CD11b positive, Ly6C negative, Ly6G negative, CD11c high, and F4/80 high (9) and based on their respective high or low expression of MHCII can be associated with tumor elimination or progression (11). Tumor infiltrating lymphoid cells from β8-LLC tumors harvested at day 14 post injection from mice treated with isotype or C6D4 (7mg/kg) on days 0 and 7 underwent multicolor cell staining and analysis. A representative gating strategy for TAM is shown for CD45+ CD11b+ Ly6g low Ly6c low F4/80+ CD11c+ MHCII high/low. The gating for granulocytic-MDSC (g-MDSC) and monocytic-MDSC (m-MDSC) are indicated.

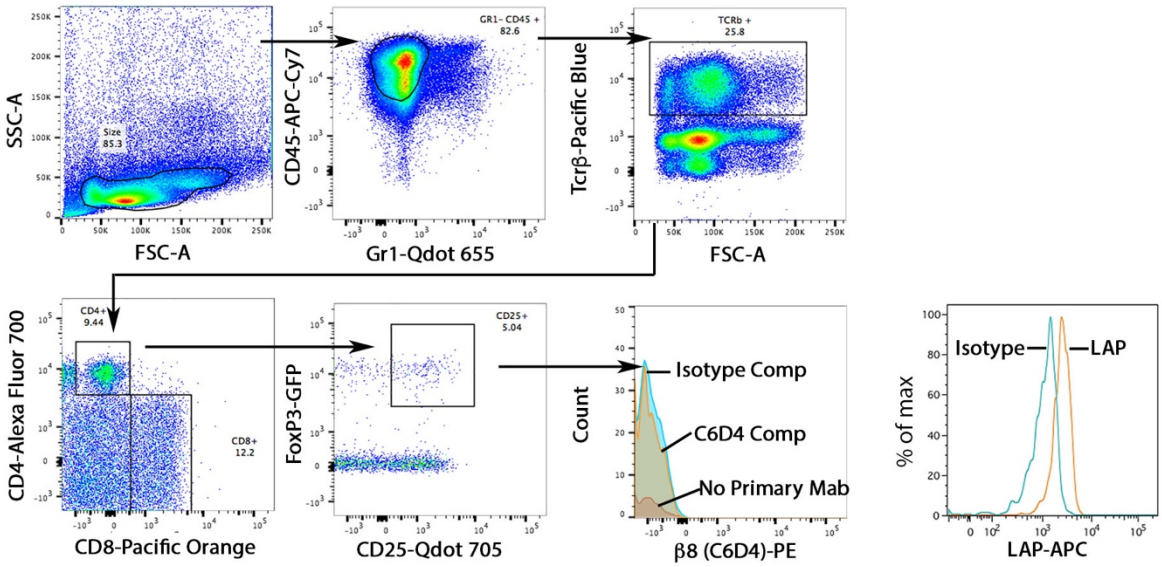

Supplemental Figure 12 TGF-β1 is expressed on the cell surface but not integrin β8 on tumor associated CD4+, Treg from FoxP3-GFP mice β8 LLC tumors were established in mice expressing GFP inserted into FoxP3 downstream of the endogenous Foxp3 STOP codon (B6.Cg-Foxp3tm2Tch/J). After tumors reached endpoint, tumor infiltrating lymphoid cells were isolated and stained for human β8 (C6D4-PE), CD45, TCRβ, CD4, CD8, Gr1, CD25 and the latency associated peptide (LAP) of TGF-β1. To determining specific staining for small amounts of cell surface β8, a 100-fold excess of unlabeled C6D4 (**C6D4 Comp**) or isotype control (**isotype comp**, anti-human β8 Mab clone B5) was added to C6D4-PE stained samples. A representative histogram overlay of isotype control and LAP stained FoxP3+CD25+ cells are shown. Shown is a representative experiment (n=3).

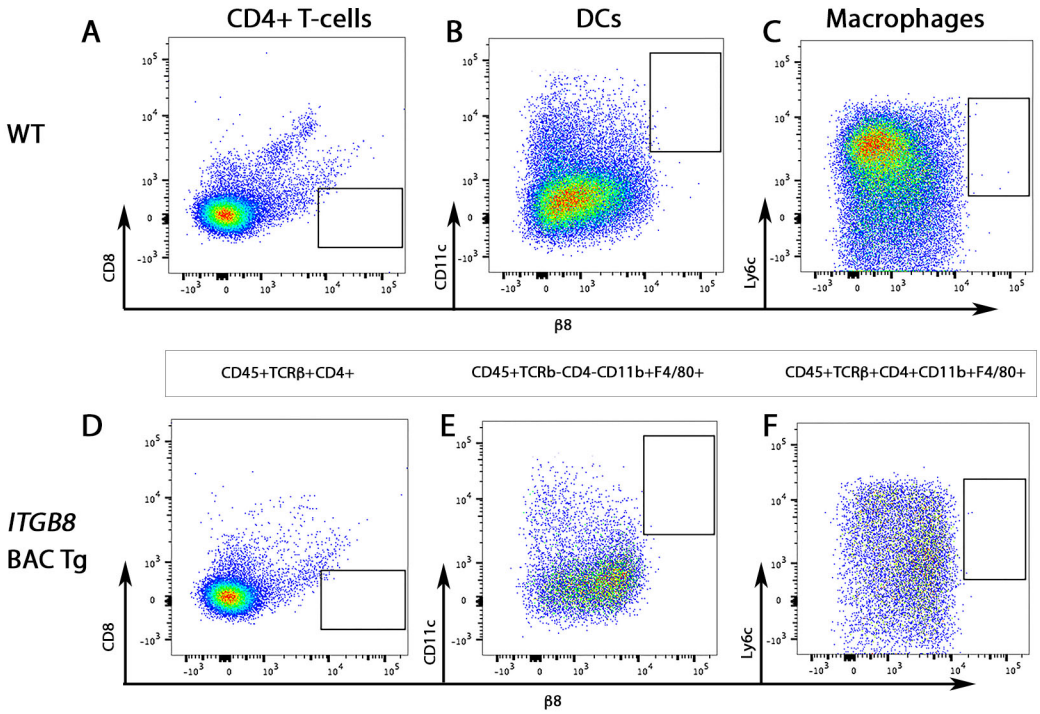

Supplemental Figure 13: The integrin β8 subunit is not expressed by tumor associated CD4+, dendritic cells, or macrophages in humanized *ITGB8* BAC transgenic mice Mice expressing human β8 under the control of 70 kb of 5' and 30 kb of 3' *ITGB8* flanking regions, respectively, were crossed to *itgb8* -/- mice to create humanized *ITGB8* mice (1). These mice were used to confirm that a highly sensitive anti-human β8 antibody could not detect β8 in immune cells. β8 LLC cells were injected into the flank of humanized *ITGB8* mice or WT mice as a control. After tumors reached endpoint (day 14), tumor infiltrating lymphoid cells were isolated and stained for human β8 (68-PE), CD45, TCRβ, CD4, CD8, CD11b, CD11c, F4/80 and Ly6c. Gating strategies are indicated in a box between panels A-C and D-F. Boxes within the panels indicate the expected location where β8 positive CD4, dendritic cells and macrophages would be expected, based on isotype controls.

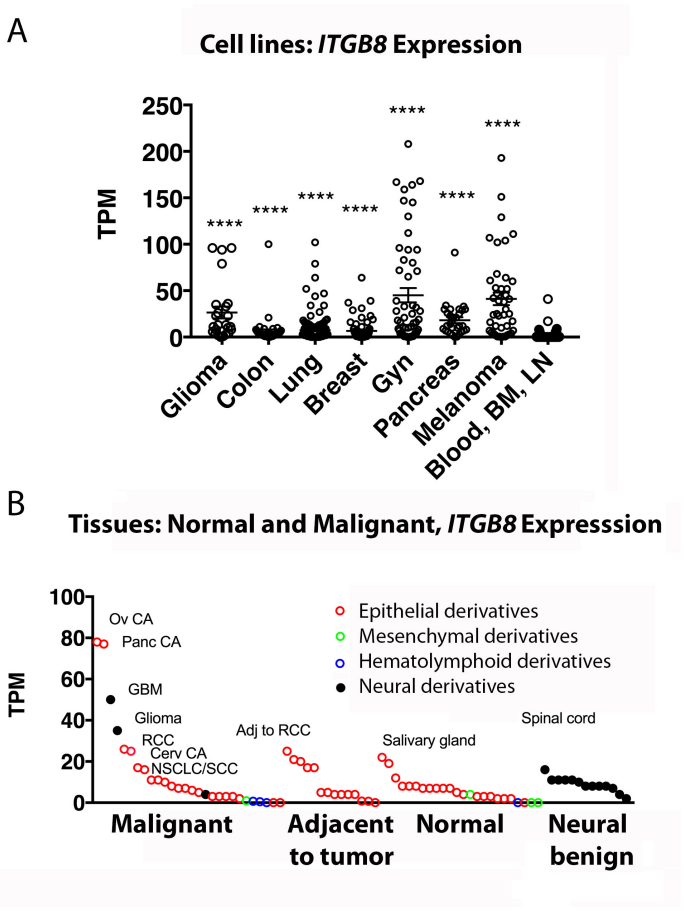

Supplemental Figure 14: Expression of *ITGB8* across various human epithelial, neural and hematogenous and lymphoid-derived malignant cell lines The EMBL-EBI expression database (https://www.ebi.ac.uk/gxa/home) was used to access commonly used human **A)** cell lines (12) and **B)** normal and tumor tissues. Reads are expressed as transcripts per million (TPM) for each **A)** cell line (glioma, n=24; colon, n=45; lung=146, breast, n=61; gynecolologic (Gyn): ovary, uterus and cervix, n=55; pancreas, n=30, melanoma, n=44, hematolymphoid (blood, bone marrow (BM), lymph node (LN), n=92) and **B**) malignant and benign tissues (hematolymphoid, mesenchymal, epithelial, neural) including bladder, brain, breast, gastrointestinal tract, kidney, liver and gall bladder, lung, head and neck, ovary, pancreas, prostate, melanoma, mesenchyme, thyroid, cervix and uterus). Color codes indicate red: epithelial derivatives; green: mesenchymal derivatives; blue, hematolymphoid derivatives; black: neural derivatives. Increased relative expression compared to blood, bone marrow and lymphoid derived cells line was determined by Kruskal-Wallis and Dunn's multiple comparison test and correlation (Pearson r) determined using Prism (V. 7.0b) ****p<0.0001

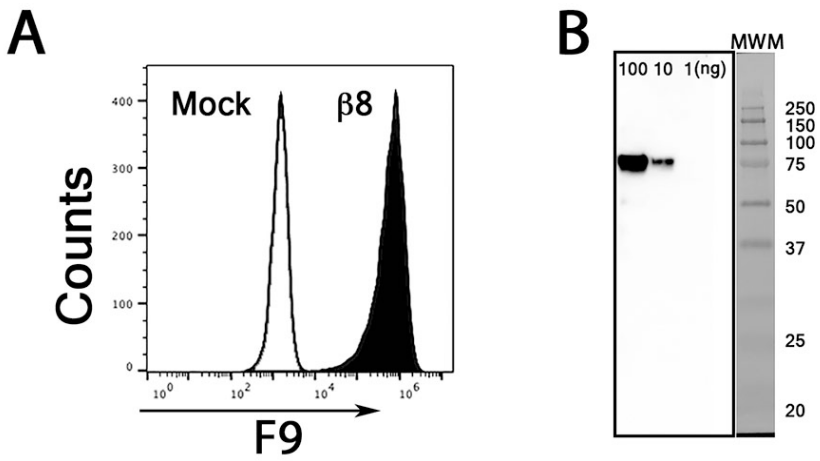

Supplemental Figure 15: Antibody clone F9 specifically recognizes the integrin β8 subunit when expressed on transfected cells and in immunoblots **A**) Transfected CHO cells either stably expressing the human β8 subunit or empty vector were stained with F9 or isotype control. Shown are histogram overlays. **B**) Recombinant αvβ8 ectodomain at various concentrations (100, 10, 1 ng/lane, non-reduced) was detected by antibody clone F9 by immunoblotting and luminescent detection. Shown are molecular weight markers (MWM). The expected migration of the β8 ectodomain is 80-90 kDa.

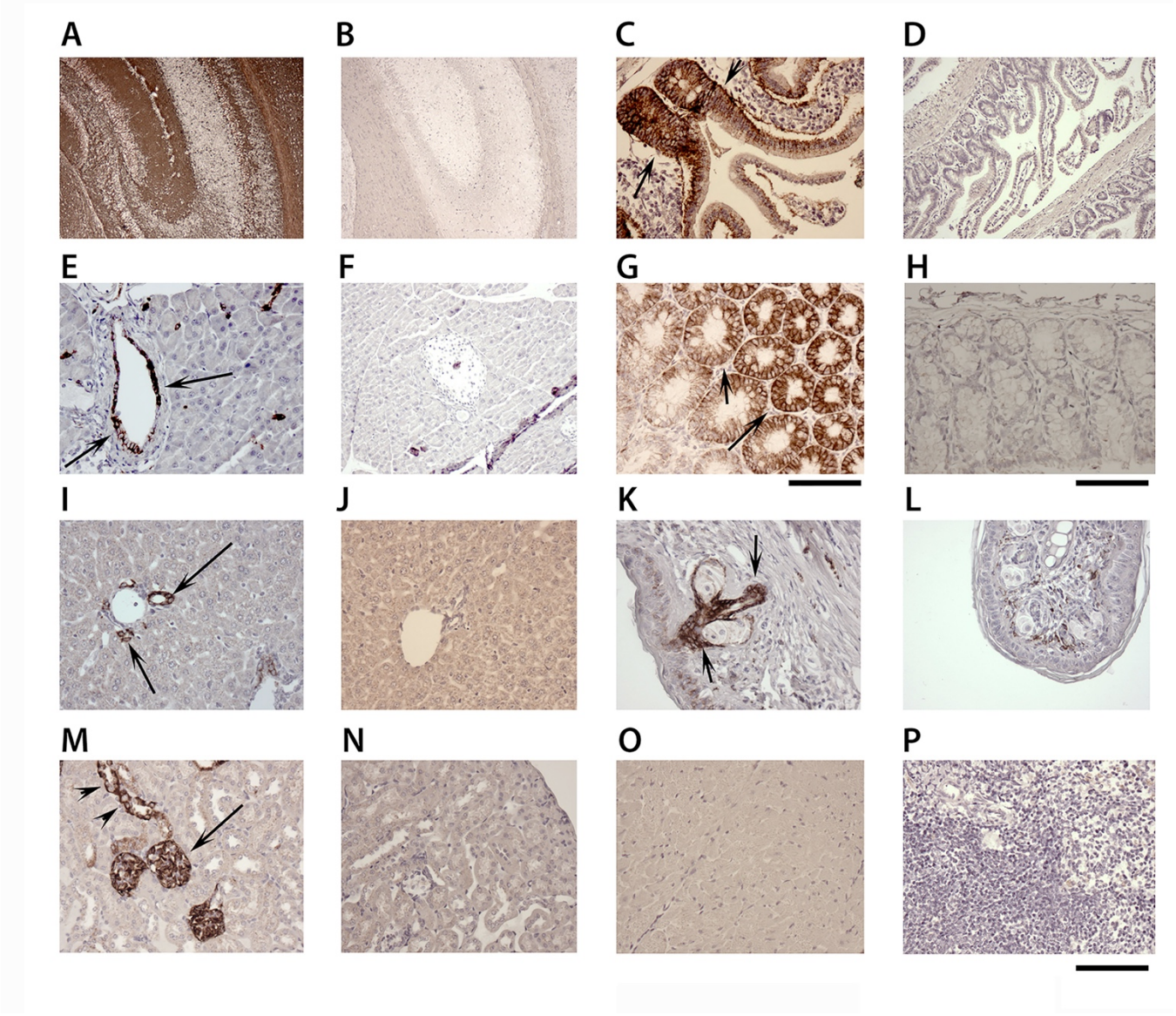

Supplemental Figure 16: Antibody clone F9 specifically recognizes the human integrin β8 subunit and not mouse β8 in brain and epithelial formalin-fixed paraffin embedded (FFPE) tissue Staining of *ITGB8* humanized mouse tissues (**A, C, E, G, I, K, M, O, P**) compared with wild-type mouse tissues (**B**, **D, F, H, J, L, N**). **A,B**) hippocampus; **C**, **D**) small bowel **E,F**) pancreas; **G,H**) colon; **I,J**) liver; **K,L**) skin; **M**, **N**) kidney, **O**) cardiac muscle **P**) spleen. Arrows indicate positively stained epithelial cells and structures. Sze bars below panel **P** = 150 μm applies to all panels except G and **H** where the bars = 75 μm.

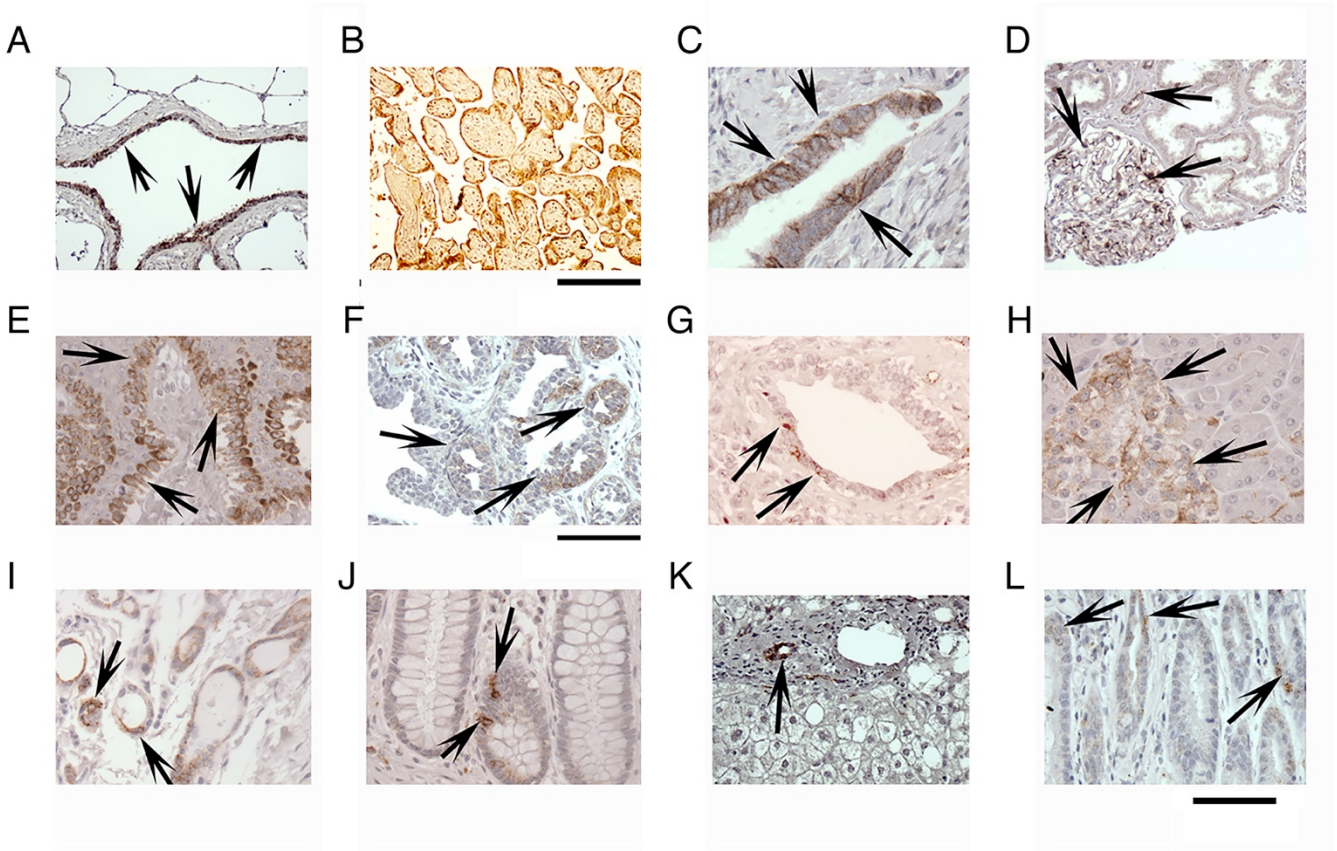

Supplemental Figure 17: **Clone F9 stains β8 in normal human epithelial and neural-derived cell types. F9 immunostaining of archival FFPE tissues** **A**) lung (airway); **B**) placenta; **C**) fallopian tube; **D**) kidney; **E**) skin; **F**) breast; **G**) pancreatic duct; **H**) pancreatic islet; **I**) prostate; **J**) Colon; **K**) liver bile duct; **L**) stomach. Arrows indicate positively stained cells and structures. 75 μm size bar in **L** refers to all panels except **B** and **F** where it represents 150 μm.

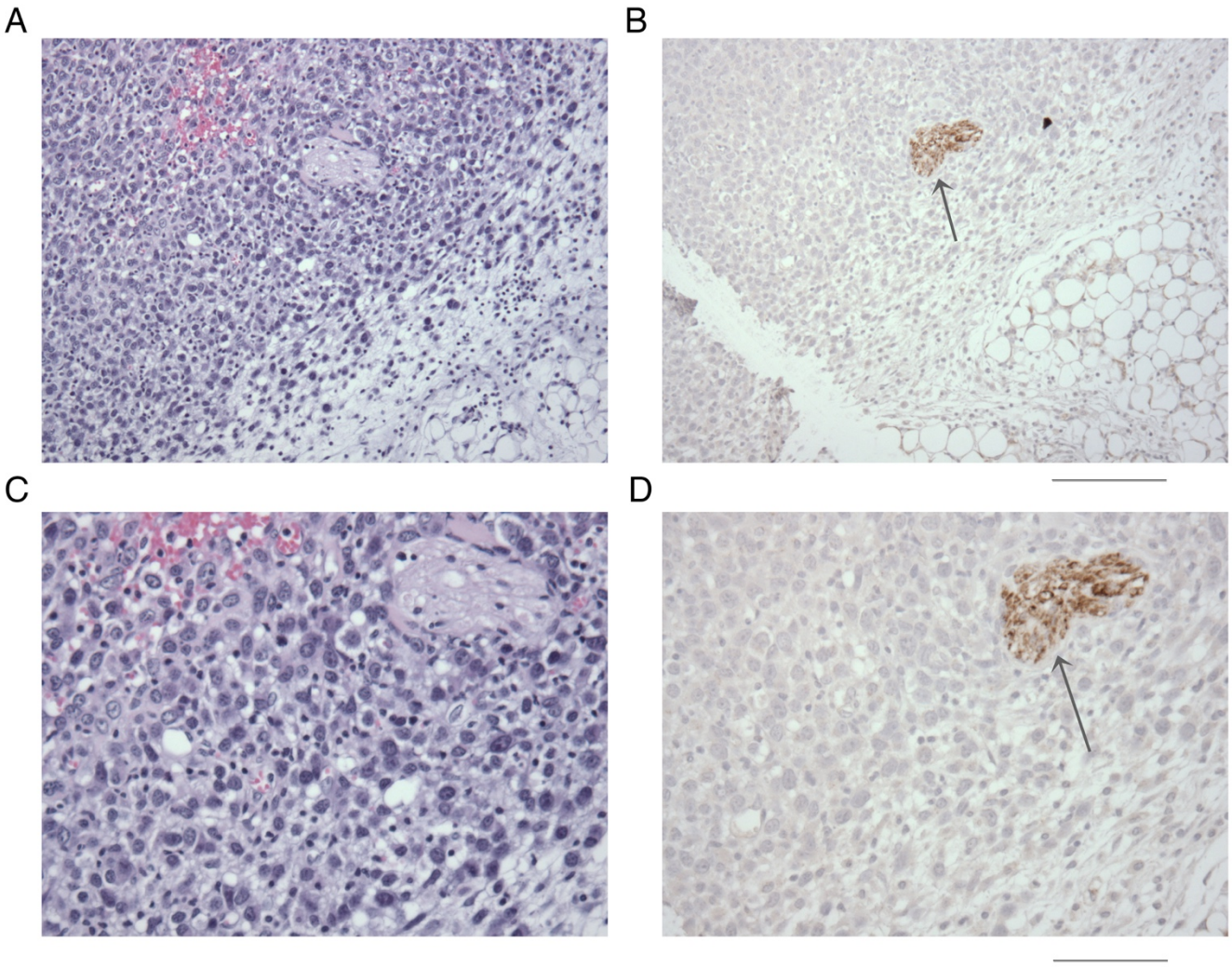

Supplemental Figure 18: **Clone F9 does not stain β8 in stromal or immune cells in LLC tumors growing in humanized *ITGB8* BAC transgenic mice** WT LLC cells were injected in the flanks of *ITGB8* BAC transgenic mice. After tumors reached 1000 mm^3 they were removed including the stromal surrounding the tumor and were formalin fixed and paraffin embedded. Sections were stained with anti-β8, clone F9 which recognizes a human-specific epitope and thus will only recognize human β8 expressing host cells and not WT LLC cells which form the tumor and do not express β8. Shown in **A, C** is a photomicrograph of an H&E stained section taken at 200X (**A**) and 400X (**C**) magnification and a photomicrograph of a F9 immunostained section taken at 200X magnification (**B**), and 400X magnification (**D**), illustrating that the only structure or cell type stained is a nerve (arrow) and no other host stromal or immune cells. **A, B**) Bar = 150 μm, **C, D**) Bar = 75 μm

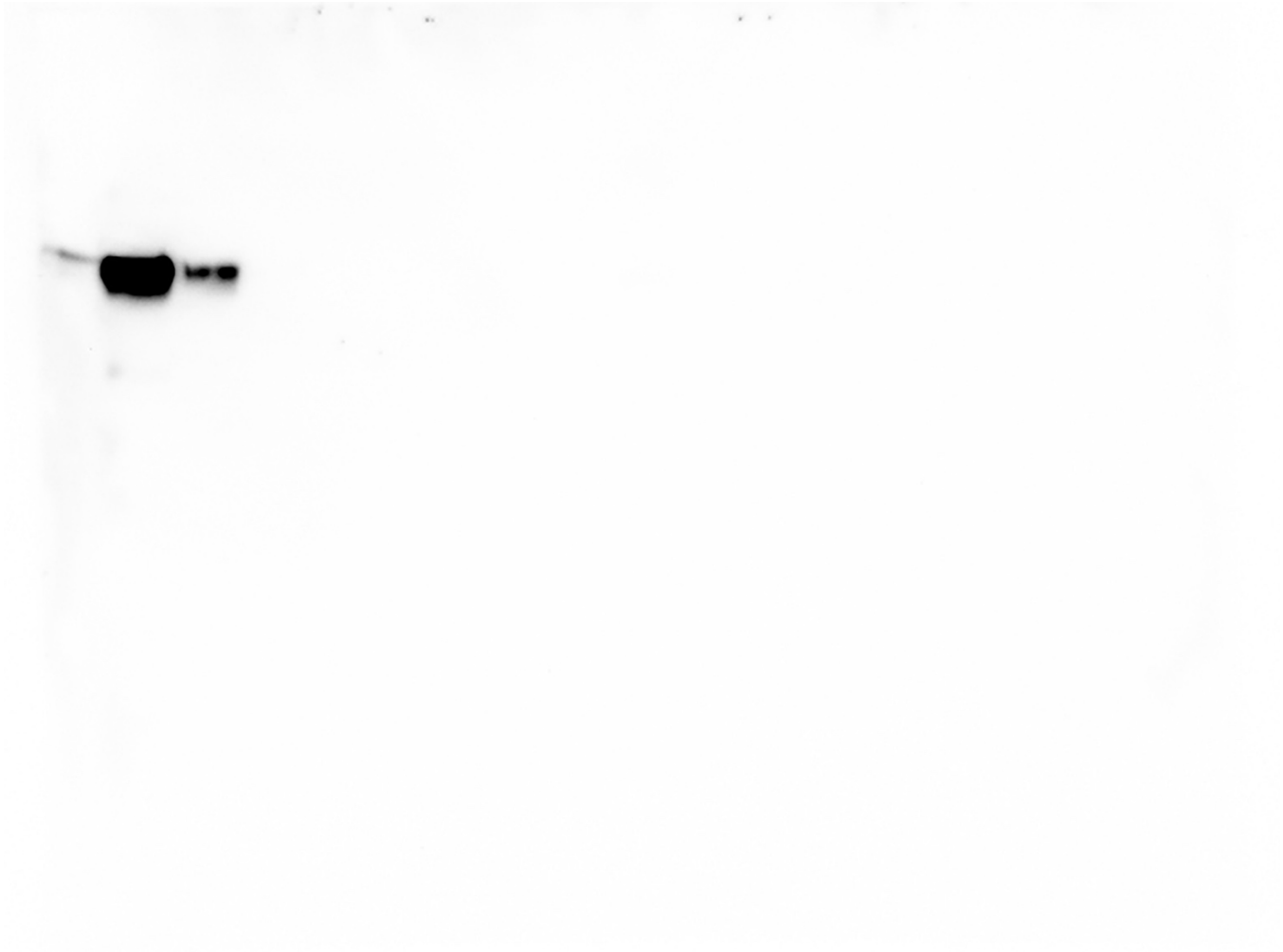

Supplemental Figure 19: **Full uncropped unedited immunoblot photomicrograph used for Supplemental Figure 15** Shown is a photomicrograph of the entire immunoblot of purified secreted αvβ8 detected with anti-β8, clone F9. Lanes 2 and 3 are cropped and shown in **Supplemental Figure 15**. A faint band in lane 1 represents sample spill-over.

Macrophages

Ensemble ID	Gene Name	log2Fold Change±1	pvalue	Padj (<0.005)	GeneDescription	MacC6D4 readcount	MacSV5 readcount	MacC6D4_ fpkm	MacSV5_ fpkm
ENSMUSG 00000040284	*Gzmg*	4.4021	4.54E-12	1.60E-07	granzyme_G	117	6	6.653203313	0.348867302
ENSMUSG 00000030147	*Clec4b1*	2.4964	1.40E-06	0.0022405	C-type_lectin_domain_family_4_ member_b1	128	25	8.84539412	1.766490518
ENSMUSG 00000055170	*Ifng*	2.4342	1.58E-06	0.0024205	interferon_gamma	147	30	6.295335516	1.313671822
ENSMUSG 00000059256	*Gzmd*	2.5743	7.39E-08	0.0004234	granzyme_D	275	51	14.74566885	2.796185904
ENSMUSG 00000016498	*Pdcd1lg2*	2.7905	1.58E-09	2.78E-05	programmed_cell_death_1_ligand_2	557	89	17.50242033	2.859545454
ENSMUSG 00000004814	*Ccl24*	2.0524	3.81E-06	0.0044784	chemokine_(C-C_motif)_ligand_24	555	148	22.25609069	6.068504774
ENSMUSG 00000031443	*F7*	2.2007	4.51E-07	0.0012243	coagulation_factor_VII	1508	363	41.93057021	10.32048567
ENSMUSG 00000040809	*Chil3*	2.0265	2.80E-06	0.0036324	chitinase-like_3	1642	446	55.14972479	15.3168387
ENSMUSG 00000046908	*Ltb4r1*	2.1012	1.21E-06	0.0021412	leukotriene_B4_receptor_1	1768	456	65.55839362	17.28920281
ENSMUSG 00000031444	*F10*	1.9891	3.52E-06	0.0042793	coagulation_factor_X	3049	850	62.96589652	17.9486164
ENSMUSG 00000037868	*Egr2*	2.2846	1.33E-07	0.00052299	early_growth_response_2	3566	810	62.16779412	14.43887049
ENSMUSG 00000029417	*Cxcl9*	2.1333	7.17E-07	0.0016872	chemokine_(C-X-C_motif)_ligand_9	3742	944	66.58347587	17.17507956
ENSMUSG000 00061100	*Retnla*	2.1309	7.05E-07	0.0016872	resistin_like_alpha	3811	963	329.4174351	85.11341245
ENSMUSG 00000049723	*Mmp12*	2.2281	2.29E-07	0.00073447	matrix_metallopeptidase_12	4978	1176	57.51322608	13.89262272
ENSMUSG 00000040950	*Mgl2*	2.08	1.18E-06	0.0021412	macrophage_galactose_N-acetyl-galactosamine_specific_lectin_2	5902	1545	186.5908163	49.94403504
ENSMUSG 00000018927	*Ccl6*	1.9914	2.88E-06	0.0036324	chemokine_(C-C_motif)_ligand_6	28824	8024	1034.666942	294.5108694
ENSMUSG 00000001506	*Col1a1*	-2.0178	2.42E-06	0.0032867	collagen_type_I_alpha_1	965	4326	8.411654701	38.55713194
ENSMUSG 00000042436	*Mfap4*	-2.1444	1.74E-06	0.0025623	microfibrillar-associated_protein_4	117	573	3.416814583	17.11016728
ENSMUSG 00000027750	*Postn*	-2.1945	1.09E-06	0.0021292	periostin_osteoblast_specific_factor	113	573	1.340601497	6.950882737
ENSMUSG 00000052316	*Lrrc15*	-2.3483	8.30E-07	0.0017525	leucine_rich_repeat_containing_15	51	288	0.496460238	2.866624884
ENSMUSG 00000028364	*Tnc*	-2.3635	1.18E-07	0.00051862	tenascin_C	163	929	1.185690166	6.909767122
ENSMUSG 00000031375	*Bgn*	-2.4284	8.40E-08	0.0004234	biglycan	110	656	2.132756905	13.00518679
ENSMUSG 00000042254	*Cilp*	-2.457	2.39E-08	0.00019502	cartilage_intermediate_layer_protein_ nucleotide_pyrophosphohydrolase	315	1915	3.920644268	24.371359
ENSMUSG 00000073599	*Ecscr*	-2.4857	1.94E-06	0.002731	endothelial_cell_surface_expressed_ chemotaxis_and_apoptosis_regulator	22	137	1.020813269	6.499923962
ENSMUSG000 00095079	*Igha*	-2.6643	8.45E-07	0.0017525	immunoglobulin_heavy_constant_alpha	18	127	0.899830652	6.49166473
ENSMUSG 00000021260	*Hhipl1*	-3.4608	1.39E-08	0.00016323	hedgehog_interacting_protein-like_1	9	111	0.178584433	2.252102491

β8 LLC cells

ID	Gene Name	log2Fold Change±1	pvalue	padj<0.005	GeneDescription	LLCC6D4_ readcount	LLCSV5_r eadcount	LLCC6D4_fpkm	LLCSV5_fpkm
None									

CD8+ T-cells

ID	Gene Name	log2Fold Change±1	pvalue	padj <0.005	GeneDescription	CD8C6D4_ readcount	CD8Sv5_re adcount	CD8C6D4_fpkm	CD8Sv5_fpkm
ENSMUSG 00000022226	*Mcpt2*	-2.8907	3.72E-10	4.38E-06	mast_cell_protease_2	96	665	5.36092199	41.52856181
ENSMUSG 00000076596	*Igkv3-10*	-3.4207	2.17E-10	3.83E-06	immunoglobulin_kappa_variable_3-10	18	181	2.741637247	30.82996649
ENSMUSG 00000095583	*Ighv14-2*	-3.4875	4.43E-12	1.56E-07	immunoglobulin_heavy_variable_14-2	34	357	5.252418049	61.67449121

CD4+ T-cells

ID	Gene Name	log2Fold Change±1	pvalue	padj<0.005	GeneDescription	CD4C6D4_ readcount	CD4Sv5_ readcount	CD4C6D4_fpkm	CD4Sv5_fpkm
ENSMUSG 00000076613	*Ighg2b*	-2.3543	3.19E-07	0.00093823	immunoglobulin_heavy_constant_ gamma_2B	86	436	4.905970515	25.53580661
ENSMUSG 00000069919	*Hba-a1*	-2.5196	2.08E-08	0.00010457	hemoglobin_alpha_adult_chain_1	145	824	11.95194766	69.73238209
ENSMUSG 00000052305	*Hbb-bs*	-2.6176	7.81E-09	5.51E-05	hemoglobin_beta_adult_s_chain	120	730	8.886883876	55.50444039
ENSMUSG 00000073940	*Hbb-bt*	-3.0793	2.32E-07	0.00074436	hemoglobin_beta_adult_t_chain	11	93	0.901540448	7.825499874
ENSMUSG 00000022226	*Mcpt2*	-5.1149	3.58E-19	1.26E-14	mast_cell_protease_2	12	416	0.712048986	25.34303165

Supplemental Table 2: Significantly differentially expressed genes

Macrophages	**Up**							
Category	ID	Description	GeneRatio	BgRatio[4]	pvalue	padj	geneID	Count>3
BP[1]	GO:0030595	leukocyte chemotaxis	5/15	190/20349	1.87E-07	0.000139988	*Ccl24/Ccl6/Cxcl9/F7/Ifng*	5
BP	GO:0060326	cell chemotaxis	5/15	258/20349	8.53E-07	0.000318655	*Ccl24/Ccl6/Cxcl9/F7/Ifng*	5
BP	GO:0050900	leukocyte migration	5/15	303/20349	1.88E-06	0.000468595	*Ccl24/Ccl6/Cxcl9/F7/Ifng*	5
BP	GO:0019221	cytokine-mediated signaling pathway	5/15	331/20349	2.90E-06	0.000541977	*Ccl24/Ccl6/Cxcl9/Mmp12/Ifng*	5
BP	GO:0048247	lymphocyte chemotaxis	3/15	49/20349	5.85E-06	0.000774444	*Ccl24/Ccl6/Cxcl9*	3
BP	GO:0070098	chemokine-mediated signaling pathway	3/15	50/20349	6.22E-06	0.000774444	*Ccl24/Ccl6/Cxcl9*	3
BP	GO:0071346	cellular response to interferon-gamma	3/15	70/20349	1.72E-05	0.001837581	*Ccl24/Ccl6/Ifng*	3
BP	GO:0072676	lymphocyte migration	3/15	81/20349	2.67E-05	0.002493937	*Ccl24/Ccl6/Cxcl9*	3
BP	GO:0030593	neutrophil chemotaxis	3/15	87/20349	3.31E-05	0.002646226	*Ccl24/Ccl6/Ifng*	3
BP	GO:0034341	response to interferon-gamma	3/15	89/20349	3.54E-05	0.002646226	*Ccl24/Ccl6/Ifng*	3
BP	GO:1990266	neutrophil migration	3/15	103/20349	5.48E-05	0.003723133	*Ccl24/Ccl6/Ifng*	3
BP	GO:0071621	granulocyte chemotaxis	3/15	108/20349	6.32E-05	0.00393109	*Ccl24/Ccl6/Ifng*	3
BP	GO:0097530	granulocyte migration	3/15	126/20349	9.99E-05	0.005739542	*Ccl24/Ccl6/Ifng*	3
BP	GO:0002687	positive regulation of leukocyte migration	3/15	133/20349	0.000117259	0.006256631	*Ccl24/Cxcl9/F7*	3
BP	GO:0097529	myeloid leukocyte migration	3/15	176/20349	0.000268088	0.012473238	*Ccl24/Ccl6/Ifng*	3
BP	GO:0002685	regulation of leukocyte migration	3/15	179/20349	0.000281738	0.012473238	*Ccl24/Cxcl9/F7*	3
BP	GO:0030335	positive regulation of cell migration	4/15	458/20349	0.000283862	0.012473238	*Ccl24/Cxcl9/F7/Ifng*	4
BP	GO:2000147	positive regulation of cell motility	4/15	476/20349	0.000328755	0.013643339	*Ccl24/Cxcl9/F7/Ifng*	4
BP	GO:0051272	positive regulation of cellular component movement	4/15	490/20349	0.000367052	0.014430939	*Ccl24/Cxcl9/F7/Ifng*	4
BP	GO:0051607	defense response to virus	3/15	202/20349	0.000401559	0.014549765	*Cxcl9/Mmp12/Ifng*	3
BP	GO:0009615	response to virus	3/15	245/20349	0.000704783	0.021936361	*Cxcl9/Mmp12/Ifng*	3
BP	GO:0032103	positive regulation of response to external stimulus	3/15	268/20349	0.000914094	0.027313142	*Ccl24/Cxcl9/F7*	3
BP	GO:0050678	regulation of epithelial cell proliferation	3/15	321/20349	0.001537087	0.039593236	*Ccl24/Mmp12/Ifng*	3
BP	GO:0042060	wound healing	3/15	351/20349	0.001984594	0.044923997	*F7/F10/Mmp12*	3
MF[2]	GO:0008009	chemokine activity	3/17	39/20291	4.38E-06	0.000181786	*Ccl24/Ccl6/Cxcl9*	3
MF	GO:0042379	chemokine receptor binding	3/17	52/20291	1.05E-05	0.000181786	*Ccl24/Ccl6/Cxcl9*	3
MF	GO:0004252	serine-type endopeptidase activity	4/17	188/20291	1.55E-05	0.000181786	*F7/F10/Gzmg/Gzmd*	4
MF	GO:0004175	endopeptidase activity	5/17	430/20291	2.09E-05	0.000181786	*F7/F10/Gzmg/Mmp12/Gzmd*	5
MF	GO:0048018	receptor ligand activity	5/17	451/20291	2.63E-05	0.000181786	*Ccl24/Ccl6/Cxcl9/Ifng/Retnla*	5
MF	GO:0005125	cytokine activity	4/17	216/20291	2.67E-05	0.000181786	*Ccl24/Ccl6/Cxcl9/Ifng*	4
MF	GO:0008236	serine-type peptidase activity	4/17	217/20291	2.71E-05	0.000181786	*F7/F10/Gzmg/Gzmd*	4
MF	GO:0017171	serine hydrolase activity	4/17	222/20291	2.97E-05	0.000181786	*F7/F10/Gzmg/Gzmd*	4
MF	GO:0030545	receptor regulator activity	5/17	484/20291	3.69E-05	0.000200987	*Ccl24/Ccl6/Cxcl9/Ifng/Retnla*	5
MF	GO:0005126	cytokine receptor binding	4/17	285/20291	7.85E-05	0.000384715	*Ccl24/Ccl6/Cxcl9/Ifng*	4
MF	GO:0001664	G-protein coupled receptor binding	3/17	270/20291	0.001379912	0.005634639	*Ccl24/Ccl6/Cxcl9*	3
Macrophages	**Down**							
Category	ID	Description	GeneRatio	BgRatio	pvalue	padj	geneID	Count >3
BP	GO:0030335	positive regulation of cell migration	4/11	458/20349	7.37E-05	0.007781287	*Col1a1/Postn/Ednra/Lrrc15*	4
BP	GO:2000147	positive regulation of cell motility	4/11	476/20349	8.56E-05	0.007781287	*Col1a1/Postn/Ednra/Lrrc15*	4
BP	GO:0051272	positive regulation of cellular component movement	4/11	490/20349	9.58E-05	0.007781287	*Col1a1/Postn/Ednra/Lrrc15*	4
BP	GO:0030198	extracellular matrix organization	3/11	206/20349	0.000158897	0.007781287	*Col1a1/Postn/Mfap4*	3
BP	GO:0043062	extracellular structure organization	3/11	207/20349	0.000161186	0.007781287	*Col1a1/Postn/Mfap4*	3
BP	GO:0001649	osteoblast differentiation	3/11	209/20349	0.000165828	0.007781287	*Col1a1/Igfbp5/Tnc*	3
BP	GO:0071214	cellular response to abiotic stimulus	3/11	217/20349	0.000185269	0.007781287	*Col1a1/Ednra/Mfap4*	3
BP	GO:0104004	cellular response to environmental stimulus	3/11	217/20349	0.000185269	0.007781287	*Col1a1/Ednra/Mfap4*	3

BP	GO:0071496	cellular response to external stimulus	3/11	226/20349	0.000208849	0.008040669	*Col1a1/Postn/Ednra*	3
BP	GO:0007162	negative regulation of cell adhesion	3/11	252/20349	0.000287714	0.010224916	*Col1a1/Postn/Tnc*	3
BP	GO:0001503	ossification	3/11	378/20349	0.000939142	0.021323137	*Col1a1/Igfbp5/Tnc*	3
CC[3]	GO:0005578	proteinaceous extracellular matrix	6/11	348/20585	9.62E-09	2.60E-07	*Col1a1/Postn/Tnc/Bgn/Cilp/Mfap4*	6
CC	GO:0044420	extracellular matrix component	3/11	129/20585	3.82E-05	0.000516248	*Col1a1/Tnc/Mfap4*	3
MF	GO:0001968	fibronectin binding	3/9	30/20291	2.44E-07	5.60E-06	*Igfbp5/Tnc/Lrrc15*	3
β8 LLC cells	**Up**							
Category	ID	Description	GeneRatio	BgRatio	pvalue	padj	geneID	Count>3
None								
β8 LLC cells	**Down**							
Category	ID	Description	GeneRatio	BgRatio	pvalue	padj	geneID	Count>3
None								
CD8+ T-cells	**Up**							
Category	ID	Description	GeneRatio	BgRatio	pvalue	padj	geneID	Count>3
None								
CD8+ T-cells	**Down**							
Category	ID	Description	GeneRatio	BgRatio	pvalue	padj	geneID	Count>3
None								
CD4+ T-cells	**Up**							
Category	ID	Description	GeneRatio	BgRatio	pvalue	padj	geneID	Count>3
CD4+ T-cells	**Down**							
Category	ID	Description	GeneRatio	BgRatio	pvalue	padj	geneID	Count>3
BP	GO:0048821	erythrocyte development	3/4	33/20349	1.55E-08	3.73E-07	*Hbb-b1/Hbb-b2/Hba-a1*	3
BP	GO:0061515	myeloid cell development	3/4	68/20349	1.42E-07	1.71E-06	*Hbb-b1/Hbb-b2/Hba-a1*	3
BP	GO:0030218	erythrocyte differentiation	3/4	117/20349	7.38E-07	5.81E-06	*Hbb-b1/Hbb-b2/Hba-a1*	3
BP	GO:0034101	erythrocyte homeostasis	3/4	128/20349	9.68E-07	5.81E-06	*Hbb-b1/Hbb-b2/Hba-a1*	3
BP	GO:0002262	myeloid cell homeostasis	3/4	161/20349	1.93E-06	9.28E-06	*Hbb-b1/Hbb-b2/Hba-a1*	3
BP	GO:0048872	homeostasis of number of cells	3/4	294/20349	1.18E-05	4.05E-05	*Hbb-b1/Hbb-b2/Hba-a1*	3
BP	GO:0030099	myeloid cell differentiation	3/4	373/20349	2.41E-05	7.23E-05	*Hbb-b1/Hbb-b2/Hba-a1*	3
CC	GO:0044445	cytosolic part	5/6	240/20585	1.23E-09	1.11E-08	*Hbb-b1/Hbb-b2/Hbb-bs/Hba-a1/Hbb-bt*	5
CC	GO:0072562	blood microparticle	5/6	107/20585	2.70E-06	1.22E-05	*Hbb-bs/Hba-a1/Hbb-bt*	3
MF	GO:0019825	oxygen binding	5/6	19/20291	8.22E-12	1.07E-10	*Hbb-b2/Hbb-bs/Hba-a1/Hbb-bt*	4
MF	GO:0004601	peroxidase activity	5/6	41/20291	1.52E-07	8.21E-07	*Hbb-bs/Hba-a1/Hbb-bt*	3
MF	GO:0016684	oxidoreductase activity, acting on peroxide as acceptor	5/6	44/20291	1.89E-07	8.21E-07	*Hbb-bs/Hba-a1/Hbb-bt*	3
MF	GO:0016209	antioxidant activity	5/6	79/20291	1.13E-06	3.66E-06	*Hbb-bs/Hba-a1/Hbb-bt*	3

[1]CF, Biologic Function
[2]MF, Molecular Function
[3]CC, Cellular Component

Supplemental Table 2: Gene Ontology Enrichment

Supplemental References:

1. Minagawa S, Lou J, Seed RI, Cormier A, Wu S, Cheng Y, et al. Selective targeting of TGF-beta activation to treat fibroinflammatory airway disease. *Sci Transl Med.* 2014;6(241):241ra79.
2. Rimm DL, Han G, Taube JM, Yi ES, Bridge JA, Flieder DB, et al. A Prospective, Multi-institutional, Pathologist-Based Assessment of 4 Immunohistochemistry Assays for PD-L1 Expression in Non-Small Cell Lung Cancer. *JAMA Oncol.* 2017;3(8):1051-8.
3. Roach C, Zhang N, Corigliano E, Jansson M, Toland G, Ponto G, et al. Development of a Companion Diagnostic PD-L1 Immunohistochemistry Assay for Pembrolizumab Therapy in Non-Small-cell Lung Cancer. *Appl Immunohistochem Mol Morphol.* 2016;24(6):392-7.
4. Kim H, Kwon HJ, Park SY, Park E, and Chung JH. PD-L1 immunohistochemical assays for assessment of therapeutic strategies involving immune checkpoint inhibitors in non-small cell lung cancer: a comparative study. *Oncotarget.* 2017;8(58):98524-32.
5. Mazzocca A, Fransvea E, Lavezzari G, Antonaci S, and Giannelli G. Inhibition of transforming growth factor beta receptor I kinase blocks hepatocellular carcinoma growth through neo-angiogenesis regulation. *Hepatology.* 2009;50(4):1140-51.
6. Casazza A, Laoui D, Wenes M, Rizzolio S, Bassani N, Mambretti M, et al. Impeding macrophage entry into hypoxic tumor areas by Sema3A/Nrp1 signaling blockade inhibits angiogenesis and restores antitumor immunity. *Cancer Cell.* 2013;24(6):695-709.
7. Xiong JP, Stehle T, Diefenbach B, Zhang R, Dunker R, Scott DL, et al. Crystal structure of the extracellular segment of integrin alpha Vbeta3. *Science.* 2001;294(5541):339-45.
8. Su X, Esser AK, Amend SR, Xiang J, Xu Y, Ross MH, et al. Antagonizing Integrin beta3 Increases Immunosuppression in Cancer. *Cancer research.* 2016;76(12):3484-95.
9. Franklin RA, Liao W, Sarkar A, Kim MV, Bivona MR, Liu K, et al. The cellular and molecular origin of tumor-associated macrophages. *Science.* 2014;344(6186):921-5.
10. Desombere I, Meuleman P, Rigole H, Willems A, Irsch J, and Leroux-Roels G. The interferon gamma secretion assay: a reliable tool to study interferon gamma production at the single cell level. *J Immunol Methods.* 2004;286(1-2):167-85.
11. Wang B, Li Q, Qin L, Zhao S, Wang J, and Chen X. Transition of tumor-associated macrophages from MHC class II(hi) to MHC class II(low) mediates tumor progression in mice. *BMC Immunol.* 2011;12:43.
12. Klijn C, Durinck S, Stawiski EW, Haverty PM, Jiang Z, Liu H, et al. A comprehensive transcriptional portrait of human cancer cell lines. *Nat Biotechnol.* 2015;33(3):306-12.